Conjugate heat transfer enhancement over heated blocks using airfoil deflectors

Nacera Cheriet, Hamza Amirat, Abdelkader Korichi, Guillaume Polidori

Conjugate Heat Transfer Enhancement over Heated Blocks Using Airfoil Deflectors

By

Nacera CHERIET

PhD student

Hamza AMIRAT

Lecturer

Abdelkader KORICHI,

Professor

Laboratoire de Mécanique, Physique et Modélisation Mathématique (LMP2M),

Université de Médéa,

Quartier Ain D'heb, Medea 26000, Algeria

Guillaume Polidori

MATIM, Faculté des Sciences, Université de Reims, Moulin de la Housse, 51100 Reims, France

Corresponding author : Guillaume POLIDORI guillaume.polidori@univ-reims.fr

Abstract:

This study focuses on laminar air cooling of multiple blocks mounted in a channel, with airfoils placed above the blocks and used as vortex generators. The unsteady governing equations are solved by the finite volume method using the commercial CFD code Fluent®. The flow and temperature structures are analyzed in the whole channel in both solid and fluid phases for Reynolds numbers ranging from 500 to 1800. The vortex shedding flow generated by the successive airfoils penetrates in the inert-block cavity in addition to the flow directed toward the block face, resulting in significant heat transfer. The increase in *Reynolds* number leads to the amplification of the heat transfer rate. It is found that the rate of heat transfer improvement achieved exceeds 200% for all Reynolds number values studied.

Keywords: Electronic cooling, heated blocks, heat transfer enhancement, finite volume method.

Nomenclature

a	Dimensionless x airfoil-block offset
b	Dimensionless y airfoil-block offset
c	Dimensionless airfoil length
c_p	Specific heat, $j.kg^{-1}.K^{-1}$;
f	Friction factor;
f_r	Frequency, 1/Hz;
h	Dimensionless heated block height;
H	Dimensionless channel height;
H^*	Dimensional channel height, m;
k	Thermal conductivity, $W.m^{-1}.K^{-1}$;
L_h	Dimensionless heated length
L_{in}	Dimensionless distance between the inlet and the first block front face;
L_{out}	Dimensionless distance between the outlet and the last block front face;
n	Normal coordinate;
Nu	Mean *Nusselt* number
$\overline{Nu}$	Time-averaged mean *Nusselt* number
Nu_x	Local *Nusselt* number
$\overline{Nu}_X$	Time averaged local *Nusselt* number
p	Dimensionless pressure;
Pe	Peclect number;
Pr	Prandtl number;
q''	Heat flux, $W.m^{-2}$;
Re	*Reynolds* number;
s	Dimensionless block spacing;
St	Strouhal number, eq. 17;

T Temperature, K;

t Dimensional time;

u Dimensionless x-component of velocity;

v Dimensionless y-component of velocity;

w Dimensionless block width;

x,y Dimensionless cartesian coordinates;

Greek symbols

η Index efficiency, eq. 16;

μ Dynamic viscosity, $kg.s^{-1}.m^{-1}$;

ν Kinematic viscosity of air [$m^2\ s^{-2}$]

ξ Dimensionless block peripheral distance

θ Dimensionless temperature;

ρ Density, $kg.m^{-3}$;

τ Dimensionless time;

Subscripts

0 Inlet;

f Fluid;

s Solid;

m Mean:

pp relative to the parallel plate channel.

superscripts

$*$ Dimensional;

1. Introduction:

Heat transfer from mounted blocks simulating electronic components has been the subject of interest of many works in the last decades [1-4]. Initially, these investigations studied the basic geometrical configuration of convective/conductive heat transfer from a single or an array of heated blocks attached to walls without any inserts. As technology has enhanced, systems have become more powerful,

leading to critical heat generation. Thus, the basic configuration of the block arrangement no longer allowed sufficient evacuation of the accumulated energy. Different techniques, classified as active or passive, were tested to improve heat removal. Active techniques involve insertion in the flow of moving objects like oscillating / swinging or rotating ones by external forces, consuming more energy and requiring permanent maintenance. On the contrary, passive methods do not require any additional costs. Commonly used passive techniques are fixed plates, bar cylinders and other geometrically shaped objects.

Herman and Kang [5] experimentally investigated, using the holographic interferometry technique, the heat transfer enhancement and fluid flow feature in a grooved channel with curved vanes placed at the trailing edge of the mounted part of the groove. They found that the flow bifurcates to the unstable regime at around Re=450; the flow and the swinging aspect of the flow increase heat transfer by up to 3.5 times compared to the core grooved channel. However, in turn, the pressure drop is found to increase to up five times. The same technique was studied numerically by Luviano-Ortiz et al. [6] at *Reynold numbers* up to 1000 using a steady-state scheme. They found that using a curved deflector reduces the flow stagnation rear the block leading to an enhancement in heat transfer. Lorenzini-Gutierrez [7] showed that the geometric parameters of the curved deflector have a significant effect on heat transfer, especially the radius which was a major factor. The experimental investigation carried out by Rosas et al. [8] revealed that a larger deflector at a small vertical distance from the block surface enhances the heat transfer for upstream and downstream block heat sources. However, the horizontal distance from the block trailing edge has a contrast effect. The optimal vertical position was found to be equal to the block height. Moreover, the authors confirmed the finding obtained by Herman and Kang [5] for the pressure losses. Cylinders and bars of various shapes have been used as vortex generators by many researchers. Fu and Tong [9] used an oscillating cylinder from heated blocks. They found that significant heat transfer is obtained for an oscillation frequency in the lock-in regime, and the enhancement increases with *the Reynolds* number. Yang and Chen used the same technique in a turbulent flow; they concluded that heat transfer is significantly enhanced, especially at the resonance frequency oscillation. The combined effect of pulsating flow and rotating cylinder placed on the channel centreline and between two blocks has been studied by Selimefendigil and Öztop [10]. They found that the direction of rotation of the cylinder can affect heat transfer. A clock-wise *rotation* direction enhances heat transfer on the top face of the subsequent blocks while a counter clock-wise direction enhances heat transfer on the rear face. Suh-Jenq Yang [11] proposed positioning an oscillating bar upstream of three heated obstacles in a channel. Their numerical investigation revealed that the vortices induced by the bar oscillation are advantageous to heat transfer from the blocks.

Wang and Jaluria [12] found that using a square cylinder as a vortex promoter in a channel with two protruding heat sources leads to flow bifurcation at a low *Reynolds number* about 600. The heat transfer increase is about 95% at *Re*=1000. In a series of works, Perng and co-authors [13-15] investigated the effect of installing of a solid/porous rectangular bar in the crossflow above the upstream block, on heat transfer in both laminar and turbulent convection. Their result showed that the

addition of a rectangular bar improves heat transfer, especially for the first blocks. Moreover, they showed that the bar height to width ratio has an important effect on the flow oscillation amplitude; however, the porosity has a slight impact. Hakan et al. [16] found that adding a triangular bar above the upstream block at the core channel increases heat transfer compared to the top wall position. In another investigation [17] on the same geometric form, they demonstrated that a position of the triangular bar on the top of the second block offers an optimum and uniform heat transfer which is independent of the *Reynolds* number. They also used an oblique plate above an upstream block as a vortex generator under mixed convection flow condition [18]. The results showed that a heat transfer enhancement of 39.5% could be reached for an inclination angle of 60°. Korichi et al. [19] studied the effect of oblique plates above each obstacle's rear in a periodic grooved channel. They found that a significant heat transfer enhancement can be obtained, up to 200%. A delta shape bar was used as a vortex generator over an arrangement of five heated blocks in the steady flow regime [20]. The results showed that the insertion of the vortex generator reduces the temperature within the blocks. Moreover, the authors found that the Reynolds number and vortex generator position have a significant effect on heat transfer. In a recent study [21], porous layer covering solid blocks were used to enhance heat transfer. Their findings showed that covers with high permeability or with decreasing permeability as going outside lead to a significant heat transfer increase.

From the above literature survey, it can be concluded that the passive methods using a vortex generator can be helpful in engineering systems for heat transfer enhancement purposes. However, all of the above works revealed that these techniques allow a significant increase in pressure drop that always accompanies heat transfer enhancement. In some cases, the friction can reach extreme values more than four times compared to the baseline configuration [6, 8]. Therefore, this work is in this context and investigates a new vortex generator to enhance heat exchange with moderate pressure drop in laminar forced convection flow over heated blocks simulating electronic components. The Naca 0012 airfoil model is used as vortex generators and flow deflectors. This model is used because it has a low drag coefficient due to its low curvature and smooth shape [22-25]. In addition, it offers simple construction and implementation in the computational code. The results will be of interest to researchers in the electronic cooling industry.

2. Physical model and formulation

The proposed configuration consists of a two-dimensional channel with an array of five heated blocks attached to the bottom wall. Naca airfoils are positioned above the downstream end of each block (Fig. 1). The blocks are identical, square-shaped, of side h and equidistant by a length s; a and b are the horizontal and vertical distances from the trailing corner of the block to the wing. The airfoils are of chord length c and inclined at an angle α to the horizontal. Air is considered as working fluid. It is considered Newtonian, incompressible with constant properties. The flow is assumed to be laminar with negligible viscous dissipations and free to bifurcate to the unsteady regime.

Under the above assumptions, the governing equations of mass, momentum, and energy can be written in a non-dimensional form as follows [26]:

Mass:

$$\frac{\partial u}{\partial x}+\frac{\partial u}{\partial y}=0 \tag{1}$$

x-momentum:

$$Re\frac{\partial u}{\partial \tau}+Re\left(u\frac{\partial u}{\partial x}+v\frac{\partial u}{\partial y}\right)=-\frac{\partial p}{\partial x}+\left(\frac{\partial^2 u}{\partial x^2}+\frac{\partial^2 u}{\partial y^2}\right) \tag{2}$$

y-momentum:

$$Re\frac{\partial v}{\partial \tau}+Re\left(u\frac{\partial v}{\partial x}+v\frac{\partial v}{\partial y}\right)=-\frac{\partial p}{\partial y}+\left(\frac{\partial^2 v}{\partial x^2}+\frac{\partial^2 v}{\partial y^2}\right) \tag{3}$$

Energy:

The fluid phase:

$$P_e\frac{\partial \theta_f}{\partial \tau}+P_e\left(u\frac{\partial \theta_f}{\partial x}+v\frac{\partial \theta_f}{\partial y}\right)=\left(\frac{\partial^2 \theta_f}{\partial x^2}+\frac{\partial^2 \theta_f}{\partial y^2}\right) \tag{4}$$

The solid phase:

$$\frac{\rho_s.c_{p_s}}{\rho_f.c_{p_f}}P_e\left(\frac{\partial \theta_s}{\partial t}\right)=\frac{k_s}{k_f}\left(\frac{\partial^2 \theta_s}{\partial x^2}+\frac{\partial^2 \theta_s}{\partial y^2}\right) \tag{5}$$

Non-dimensional variables (all lengths are adimensionalized with respect to the channel width H^*):

$$x=\frac{x^*}{H^*};\ y=\frac{y^*}{H^*};\ u=\frac{u^*}{u_m^*};\ v=\frac{v^*}{u_m^*};\ \theta=\frac{(T-T_0)k}{(q".H^*/k_f)};\ p=\frac{p^*.H}{\mu_f.u_m^*};\ \tau=\frac{tu_0}{H} \tag{6}$$

and the relevant non-dimensional groups are:

$$Re=\frac{\rho_f.u_m.H}{\mu_f};\ Pr=\frac{\mu_f.c_{p_f}}{K_f};\ Pe=Re.Pr \tag{7}$$

where u_m^* is the mean velocity.

The flow at the entrance is considered as a fully developed Poiseuille flow with a parabolic profile and constant temperature such as:

$$u_0=6y(1-y);v=0;\theta_{f0}=0 \tag{8}$$

The inlet and outlet lengths are rigorously chosen to avoid any negative impact on the results. Small distances can give rise to unrealistic situations, particularly in an unsteady regime for a too small outlet length. However, higher values consume more storage space; the adopted values are L_{in}=3, L_{out}=20. These parameters have been examined in previous studies [27].

At the channel walls, the no-slip condition is applied ($u=v=0$). At the outlet, all gradients are zero.

For the thermal boundary conditions, the channel walls are considered as adiabatic except at the block bases where constant heat flux is applied $q^{"} = 1$. At the solid-fluid interface, the continuity of heat flux and temperature is considered, thus:

$$\theta_f = \theta_s \ and \ k_f \frac{\partial \theta_f}{\partial n} = \ k_s \frac{\partial \theta_s}{\partial n} \tag{9}$$

Where n denotes the normal to the surface.

The heat transfer rate is quantified by the local *Nusselt* number, which represents the ratio of convection to pure conduction heat transfer in the fluid phase, defined as:

$$Nu_x = -\frac{\partial \theta}{\partial Y}\Big|_w \tag{10}$$

And the mean wall *Nusselt* number is given by:

$$Nu = \frac{1}{3.h}\int_0^{3.h} Nu_x dx \tag{11}$$

In unsteady flow, the time-averaged local *Nusselt* number is calculated by:

$$\overline{Nu_x} = \frac{1}{\Delta\tau}\int_\tau^{\tau+\Delta\tau} Nu_x \,.\, d\tau \tag{12}$$

Finally, the time-averaged mean *Nusselt* number is given by

$$\overline{Nu} = \frac{1}{3.h} = \int_0^{3.h} \overline{Nu_x}.\, dx \tag{13}$$

The friction factor is defined as:

$$f = \frac{\Delta P.2H}{\rho\frac{u_0^2}{2}L_h} \tag{14}$$

Where ΔP and $3h$ are the non-dimensional pressure losses and the exposed peripheral length of the obstacle, respectively.

In unsteady flow, the same averaging method used for the *Nusselt* number is applied for the friction coefficient:

$$\overline{f} = \frac{1}{\Delta\tau}\int_\tau^{\tau+\Delta\tau} f \,.\, d\tau \tag{15}$$

The heat transfer efficiency η is defined as the ratio between the *Nusselt* number and the friction coefficient divided by the same ratio but for a parallel plate channel without obstacles:

$$\eta = \frac{Nu/Nu_{pp}}{f/f_{pp}} \tag{16}$$

The Strouhal number characterizing the flow oscillation is defined as:

$$St = \frac{f_r H}{u_0} \tag{17}$$

Where f_r is the flow oscillation frequency.

3. Numerical Solution and Validation:

The governing equations associated with the above boundary conditions are solved by the finite volume formulation using the Ansys Fluent solver® [28-31]. The velocity-pressure link is handled by

the SIMPLE algorithm developed by Patankar [32]. The second-order upwind scheme is used to discretize convective terms, while the central second-order differencing discretization scheme is used for the diffusive terms. The domain extension method is used to control the thermophysical property change at the solid-fluid interface [33]. The calculations are performed iteratively until reaching the steady-state or the periodic flow oscillation using a time-varying solver where all residuals of independent variables will be less than 10^{-6}. A time-varying scheme is used to avoid imposing a stationary regime on an unsteady flow. The validation is made by comparison with the results (streamlines, block surface temperature and Nusselt number) of Young and Vafai for the case of one square block [34] and an array of five blocks [35] at *Re=1000* and *h=0.25* (Fig. 2 a,b,c). A good agreement is observed, the maximum error still below 3%. For grid independence, five grid sizes of 380×40, 410×70, 470×130, 500×160, and 520×180 have been tested for the whole domain (x,y) (Fig. 3). The maximum deviation in the *Nusselt* number between 500×160 nodes and 520x180 nodes is less than 0.05% at the highest value *Reynolds* number used (Re=2000). Thus, a 500×160 mesh size is considered sufficient to ensure a compromise between the accuracy of the results and the memory space used.

4. Results and discussions

As already mentioned, all calculations have been carried out in transient mode until stabilization, either towards a stationary regime or a bifurcation towards a self-assisted oscillatory flow. The results are presented either in a qualitative form (streamline patterns) or in a quantitative one (temperature fields, *Nusselt* number, ...). Calculations are made for four *Reynolds* number values Re= 500, 1000, 1800 and 2000 ensuring a laminar flow condition and covering both transient and steady-state flow regimes. For the geometrical parameters, the airfoil relative position for the block and the airfoil inclination angle are kept constant in this study and defined as follows: $a = 0.25$, $b = 0.5$, $c = 0.5$ and $\alpha = 45°$. The time-history of the u streamwise velocity component at a monitoring reference point (x=4.875, y=0.250, in Fig. 1) for *Re*=500 is shown in Fig. 4. This reference point is located in the area most sensitive to temporal variations due to airfoil or block disturbances. Starting from rest, the velocity oscillates as the fluid moves in the channel through the subsequent blocks and airfoils to converge to a value that will remain constant over time characterizing the stationary flow regime. The oscillation time corresponds to the flow's time; it depends on both the channel geometry complexity and the flow velocity. For Re=500 and in the configuration of this study, the steady state flow is reached after about a non-dimensional time τ=3.5. The flow structures and temperature field in the entire domain are shown in Fig. 5 for Re=500. When compared to the case without airfoils [19], the streamlines above the cavities are no longer horizontal; the wing deflects the current to the vertical face of the blocks. At low *Reynolds* number values, the flow around the airfoils at a large inclination angle is characterized by a stationary separation at an advanced point from the airfoil leading edge. For this value of the *Reynolds* number, the regime remains globally steady due to the confined space of the geometrical problem on the one hand and the small size of the wing compared to the domain dimensions on the other hand. Similar findings are reported in the literature [36, 37]. The airfoils deflect the flow stream to the upstream edges of the block reducing the size of the recirculation area between the blocks. This

decrease in size becomes more important as the flow moves downstream through the block channel. This direct impact reduces the temperature efficiently within the blocks; this result is most noticeable for the first blocks where the fluid temperature is even lower. A large vortex separation zone is generated downstream of the last obstacle at about 3h from the rear corner. The time history of the u-velocity component at the reference point (x=4.875, y=0.250) and the Fast-Fourier Transform (FFT) analysis of the same physical quantity for *Re*=1000 and 1800 are shown in Fig. 6. The FFT analysis is a power tool that decomposes a complex signal into individual spectral components and thereby provides frequency information about the incoming signal with respect to time. For both *Reynolds* number values, the velocity evolution after flow development where the velocity behaves almost randomly exhibits a periodic oscillatory behaviour around a mean value (Fig. 6.a and 6.c). The nondimensional time needed to reach the oscillating flow depends on the Reynolds number; it is about τ=5 for Re=1000 and τ=6.35 for Re=1800. At relatively high *Reynolds* number, the periodic displacement of the separation point gives rise to the Kelvin-Helmholtz instabilities. Increasing *Reynolds* number, flow separation from the trailing edge of the airfoils is no longer stable and no more perpetual in time. The separation point defers from the trailing edge to the leading edge of the airfoils; as it approaches the leading edge, the separation zone thick growth. A large vortex becomes unstable and split off from the airfoils giving rise to a vortex shedding scenario. At the same time, for a higher *Reynolds* number, a similar mechanism takes place on the top face of the block. The separation of viscous shear boundary above the horizontal face generates Tollmien-Schlichting instabilities. The Fast-Fourier Transform (FFT) analysis of the time history evolution of the velocity component at *Re*=1000 reveals a unique frequency of Strouhal number *St*=2.4414 (Fig. 6.b). As *Reynolds* number increases (*Re*=1800), in addition to the dominant frequency with *St1*=2.2461, a low-amplitude harmonic arises at a Strouhal number *St2* that is twice as high as the first frequency (Fig. 6.d). It is found that, for successive airfoils in a confined channel with blocks, the Strouhal number decreases linearly with increasing *Reynolds* number in the range $1000 \leq Re \leq 2000$ (Tab. 1). In all calculations, the *Reynolds* number is based on the height of the channel (H).

The flow and thermal patterns illustrated by streamlines and temperature contours during one oscillation cycle for *Reynolds* numbers Re=1000 and 1800 are shown in Figs. 7 and 8, respectively. As can be seen from these sequences, at *Reynolds* number of 1000, the unsteady motion generated by the Kelvin-Helmholtz instabilities slightly affects the flow feature in the cavities because of its low oscillation amplitude. However, at *Reynolds* number of 1800, the high amplitude periodically putsches the flow above the obstacles and in the cavities, leading to moving disturbances of the boundary layer on the top faces and substantial variations of the size of the recirculating zones. These unsteady periodic behaviours cause and amplify the onset of premature flow oscillation around the block arrangement. Boundary layer interruptions and disturbances are effective in reducing the temperature at the surface of the blocks as well as in the cavities through faster fluid regeneration. Furthermore, the airfoils redirect the streamflow downward, which accentuates the flow impact on the vertical front of each block. Downstream of the blocks, there is a strong interaction between the two waves, the one created by the airfoils and the one inherent to the viscous instability due to the block top faces. The heat transfer intensity characterized by the *Nusselt* number over the exposed block faces is depicted in

Fig. 9. As expected, the *Nusselt* number over the first block front face is the highest for all *Reynolds* numbers because it is exposed to the incoming cold flow. *Nusselt* number decreases asymptotically along the top face, followed by a sharp decrease on the rear block face. The *Reynolds* number has a moderate effect on the *Nusselt* number over the first block, except on the last portion of the rear face where the *Nusselt* number for *Re*=1800 is relatively high due to the active fluid regeneration. For the second block, the *Reynolds* number has a stunning effect on the top face. The reason is that, for this high *Reynolds value* and as can be seen from the streamlines (Fig. 8), the first airfoil generates a large amplitude vortex sweeping the subsequent face in the downstream direction, leading to removing more heat from this face. The increase in *Reynolds* number results in a substantial increase in the *Nusselt* number for the other blocks, although it remains lower than for the second one. To quantify the overall heat transfer improvement per block, a histogram comparison is performed for the three *Reynolds* Number values with and without airfoils (Fig. 10). It appears that the heat transfer improvement obtained for the first block with airfoil is about three times that of the case without airfoil, regardless the *Reynolds* number value. For the second block, the increase achieved is of the same order as that of the first at *Reynolds* 500 and 1000, but it exceeds four times at *Re*=1800. For the third and last two blocks, the increase is about 2.5 and 2 times respectively. Unfortunately, the transfer improvement obtained is not without cost; this increase is always coupled with an increased pressure drop in the system. Figure 11 points up the variation of the friction factor versus *Reynolds* number for the two cases: with and without airfoils. As can be seen, inserting airfoils above the blocks increases the friction factor by about two times. The increase in pressure drop results, in addition to the acceleration of the fluid due to the reduction of the cross-sectional area, from the action of the fluid on the airfoils and the resulting deflection of the flow. Heat transfer efficiency, represented by the ratio of heat transfer enhancement to the resulting pressure drop augmentation by the addition of airfoils, η, is depicted in Fig. 12. The efficiency for the case without airfoils is added for comparison. In this equation, the subscript *pp* refers to the parallel plate channel. It can be concluded that, in terms of efficiency, the placement of the airfoils leads to a significant improvement in heat transfer, about twice as much as the case without airfoils. Although the installation of airfoils above the blocks increases the pressure drop, the gain obtained in the heat transfer enhancement is very high, which makes it a very interesting technological solution. The heat transfer augmentation obtained by the insertion of airfoils compared to the heat transferred without airfoils at various *Reynolds* numbers for all blocks is summarised in Tab. 2. The Nusselt number is averaged over the five blocks for each case. As can be concluded, the increase is more than double in the steady-state for *Re*=500, while it exceeds two-and-a-half times in the variable state for Re=1800.

5. Conclusion:

In this paper, numerical simulations of forced convection flow over an array of heated obstacles with adjunction of successive airfoils as vortex generators are carried out. The airfoils are fixed above the blocks with a given position and tilt angle. The effect of *Reynolds* number on the flow and heat transfer is studied. The *Reynolds* number varies from 500 to 1800 to cover the two flow regimes, steady and unsteady, and to remain within the laminar flow limits. The obtained results demonstrated that the

successive airfoils shift the main flow towards the cavities contributing to the regeneration of the stagnant recirculating flow and allowing direct contact with the faces of the blocks. The presence of the airfoils causes an early bifurcation of the flow to the unsteady regime at relatively low *Reynolds* number values (Re<1000). The Strouhal number of the obtained oscillatory flow decreases with increasing *Reynolds* number. Propagating waves further improve the fluid mixing and thus attenuate its temperature, leading to a more significant increase in heat transfer.

However, the gain in heat transfer is not without cost, since it induces a significant increase in pumping power expressed by an increase in the friction coefficient.

References

1. Davalath J, Bayazitoglu Y. Forced Convection Cooling Across Rectangular Blocks. J. Heat Transfer. 1987; https://doi.org/10.1115/1.3248083

2. Menni Y, Ahmed Azzi A, Chamkha A, Enhancement of convective heat transfer in smooth air channels with wall-mounted obstacles in the flow path. J. Therm. Anal. Calorim. 2019; https://doi.org/10.1007/s10973-018-7268-x
3. Ghofrane Sekrani G, Poncet S, Proulx P. Conjugated heat transfer and entropy generation of Al2O3–water nanofluid flows over a heated wall-mounted obstacle. J. Therm. Anal. Calorim. 2019; https://doi.org/10.1007/s10973-018-7349-x

4. Yeh LT. Review of Heat Transfer Technologies in Electronic Equipment. J. Electron. Packag. 1995; https://doi.org/10.1115/1.2792113

5. Herman C, Kang E. Heat transfer enhancement in a grooved channel with curved vanes. Int. J. Heat and Mass Transfer. 2002; https://doi.org/10.1016/S0017-9310(02)00092-3

6. Luviano-Ortiz L, Hernandez-Guerrero A, Rubio-Arana C, Romero-Mendez R. Heat transfer enhancement in a horizontal channel by the addition of curved deflectors. Int. J. Heat and Mass Transfer. 2008; https://doi.org/10.1016/j.ijheatmasstransfer.2007.12.020

7. Lorenzini-Gutierrez D, Hernandez-Guerrero A, Luviano-Ortiz JL, Leon-Conejo JC, Numerical and experimental analysis of heat transfer enhancement in a grooved channel with curved flow deflectors. Appl. Therm. Eng. 2015; https://doi.org/10.1016/j.applthermaleng.2014.10.002.

8. Rosas AS, Ali RK, Abdel-Aziz AA, Elshazly KM, An experimental investigation of convective heat transfer enhancement in electronic module using curved deflector. Heat Mass Transfer. 2017; https://doi.org/10.1007/s00231-016-1863-9

9. Fu W-S, Tong B-H. Numerical investigation of heat transfer characteristics of the heated blocks in the channel with a transversely oscillating cylinder, Int. J. Heat and Mass Transfer. 2004; https://doi.org/10.1016/S0017-9310(03)00303-X

10. Selimefendigil F, Öztop HF, Numerical study and identification of cooling of heated blocks in pulsating channel flow with a rotating cylinder. Int. J. Therm. Sci. 2014; https://doi.org/10.1016/j.ijthermalsci.2014.01.010.

11. Yang S-J. A numerical investigation of heat transfer enhancement for electronic devices using an oscillating vortex generator, Num. Heat Transf. A. 2002; https://doi.org/10.1080/10407780290059549

12. Wang Q, Jaluria Y, Unsteady mixed convection in a horizontal channel with protruding heated blocks and a rectangular vortex promoter. Phys. Fluids. 2002; https://doi.org/10.1063/1.1480832

13. Perng S-W, Wu H-W. Numerical investigation of mixed convective heat transfer for unsteady turbulent flow over heated blocks in a horizontal channel. Int. J. Therm. Sci. 2008; https://doi.org/10.1016/j.ijthermalsci.2007.04.003

14. Perng S-W, Wu H-W, Jue T-C. Numerical investigation of heat transfer enhancement on a porous vortex-generator applied to a block-heated channel. Int. J. Heat and Mass Transfer. 2012; https://doi.org/10.1016/j.ijheatmasstransfer.2012.02.037

15. Perng S-W, Wu H-W, Jue T-C. Heat transfer augmentation and vortex-induced vibration in a block-heated channel, Int. J. Therm. Sci. 2014; https://doi.org/10.1016/j.ijthermalsci.2013.12.004

16. Oztop HF, Varol Y, Alnak DE. Control of heat transfer and fluid flow using a triangular bar in heated blocks located in a channel, Int. Commun. in Heat Mass Transf. 2009; https://doi.org/10.1016/j.icheatmasstransfer.2009.05.006

17. Beig SA, Mirzakhalili E, Kowsari F. Investigation of optimal position of a vortex generator in a blocked channel for heat transfer enhancement of electronic chips. Int. J. Heat Mass Transfer. 2011; https://doi.org/10.1016/j.ijheatmasstransfer.2011.05.013

18. Wu H-W, Perng S-W. Effect of an oblique plate on the heat transfer, enhancement of mixed convection over heated blocks in a horizontal channel. Int. J. Heat and Mass Transfer. 1999; https://doi.org/10.1016/S0017-9310(98)00247-6

19. Korichi A, Oufer L, Polidori G, Heat transfer enhancement in self-sustained oscillatory flow in a grooved channel with oblique plates. Int. J. Heat Mass Transfer. 2009; https://doi.org/10.1016/j.ijheatmasstransfer.2008.09.013

20. Mandal S K, Deb A, Sen D. A computational study on mixed convection with surface radiation in a channel in presence of discrete heat sources and vortex generator based on RSM. J. Therm. Anal. Calorim. 2020; https://doi.org/10.1007/s10973-020-09774-w

21. Qi B, Yuan R. Heat transfer enhancement in a two-dimensional channel with perforated rectangular blocks using multi-layered porous foam. J. Therm. Anal. Calorim. 2020; https://doi.org/10.1007/s10973-020-09620-z

22. Castelli MR, Garbo F, Benini E. Numerical investigation of laminar to turbulent boundary layer transition on a Naca 0012 airfoil for vertical-axis wind turbine applications. Wind. Eng. 2011; https://doi.org/10.1260%2F0309-524X.35.6.661

23. Kurtulus DF. On the unsteady behavior of the flow around Naca 0012 airfoil with steady external conditions at Re=1000. Int. J. Micro Air Veh. 2015; https://doi.org/10.1260%2F1756-8293.7.3.301

24. Winslow J, Otsuka H, Govindarajan B, Chopra I. Basic understanding of airfoil characteristics at low Reynolds numbers (10^4–10^5). J. Aircr. 2018; https://doi.org/10.2514/1.C034415

25. Oukassou K, El Mouhsine S, El Hajjaji A, Kharbouch B, Comparison of the power, lift and drag coefficients of wind turbine blade from aerodynamics characteristics of Naca 0012 and Naca2412. Procedia Manuf. 2019; https://doi.org/10.1016/j.promfg.2019.02.312

26. Kakaç S, Yener Y. Convective Heat Transfer 2nd Edition. CRC Press, Boca Raton, 1995

27. Korichi A., Oufer L. Numerical heat transfer in a rectangular channel with mounted obstacles on upper and lower walls. Int. J. Therm. Sci. 2005; https://doi.org/10.1016/j.ijthermalsci.2004.12.003

28. Karami S, Tashakor S, Afsari A, Hashemi-Tilehnoee M. Effect of the baffle on the performance of a micro pin fin heat sink. Thermal Sci. Eng. Prog. 2019; https://doi.org/10.1016/j.tsep.2019.100417

29. Hashemi-Tilehnoee M, Tashakor S, Dogonchi AS, Seyyed Masoud Seyyedi, Khaleghi M. Entropy generation in concentric annuli of 400 kV gas-insulated transmission line. Thermal Sci. Eng. Prog. 2020; https://doi.org/10.1016/j.tsep.2020.100614

30. Hashemi-Tilehnoee M, Sahebi N, Dogonchi AS, Seyyed Masoud Seyyedi, Tashakor S. Simulation of the dynamic behavior of a rectangular single-phase natural circulation vertical loop with asymmetric heater. Int J Heat Mass Transf. 2019; https://doi.org/10.1016/j.ijheatmasstransfer.2019.05.076

31. Hashemi-Tilehnoee M, Tashakor S, Seyyed Masoud Seyyedi, Sahebi N. Forced reflood modeling in a 2x2 rod bundle with a 90% partially blocked region. Ann. Nucl. Energy 2019; https://doi.org/10.1016/j.anucene.2019.04.019

32. Patankar SV. Numerical Heat Transfer and Fluid Flow, 1st ed. CRC, New York, USA; 1980.

33. Chen X, Han P. A note on the solution of conjugate heat transfer problems using SIMPLE-like algorithms. Int. J. Heat Fluid Flow. 2000; https://doi.org/10.1016/S0142-727X(00)00028-X

34. Young TJ and K. Vafai. Convective cooling of a heated obstacle in a channel. Int. J. Heat Mass Transfer. 1998; https://doi.org/10.1016/S0017-9310(97)00323-2

35. Young TJ., and K. Vafai, Convective flow and heat transfer in a channel containing multiple heated obstacles, Int. J. Heat Mass Transfer. 1998, https://doi.org/10.1016/S0017-9310(98)00014-3

36. Srinath DN, Mittal S. Optimal airfoil shapes for low Reynolds number flows. Int. J. Numer. Methods Fluids. 2009; https://doi.org/10.1002/fld.1960

37. Huang RF, Linf CL. Vortex shedding and shear-layer instability of wing at low-Reynolds numbers, AIAA J. 1995; https://doi.org/10.2514/3.12561

Figures captions:

Fig. 1: Schematic diagram of the physical domain.

Fig. 2: Computation validation by comparison with the results of Young and Vafai [34, 35]: **(a)** streamlines, **(b)** obstacle surface temperature and **(c)** local Nusselt number.

Fig.3: Grid independence: **(a)** detail of the mesh whose size is 500x160 for the whole domain around 5 blocks **(b)** *Nusselt* number according to different grid sizes**.**

Fig. 4: u-velocity history at (x=4.875, y=0.250) for Re=500.

Fig. 5: Streamlines and isotherms field for Re=500.

Fig. 6: The u-velocity history and FFT analysis for Re=1000 and 1800.

Fig. 7: Streamlines and isotherms contours during one time period for Re=1000.

Fig. 8: Streamlines and isotherms contours during one time period for Re=1800.

Fig. 9: Local Nusselt number evolution over the blocks surface.

Fig. 10: Mean bloc Nusselt number at different Reynolds number values.

Fig. 11: Friction factor versus Reynolds number with and without airfoils.

Fig. 12: Heat transfer efficiency vs. Reynolds number

Tables captions:

Tab. 1: Strouhal number of the dominant frequency for different Reynolds number values.

Tab. 2: Heat transfer augmentation at different Reynolds number values.

Figures

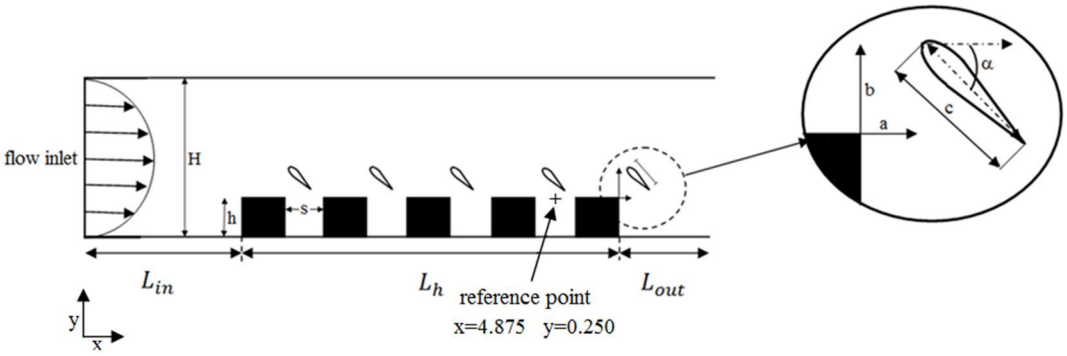

Fig. 1: Schematic diagram of the physical domain.

(a)

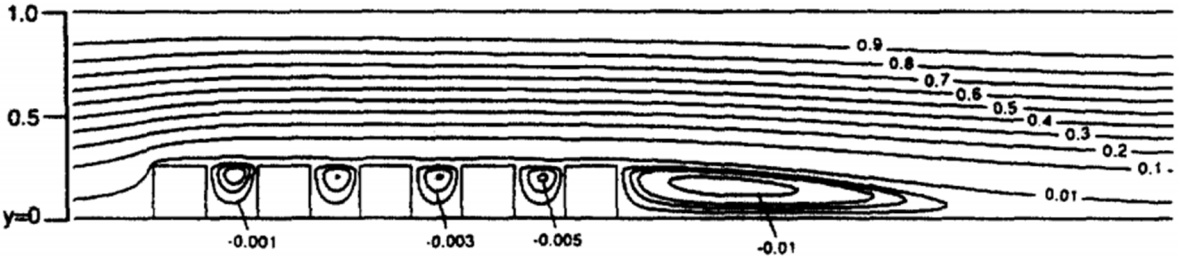

Young and Vafai [35]

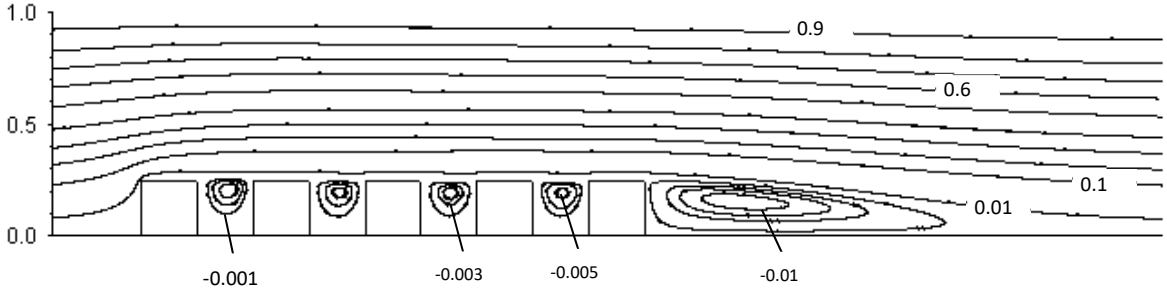

Present work

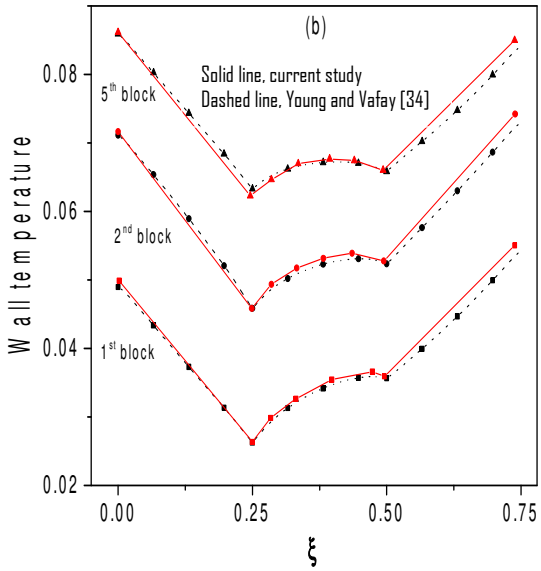

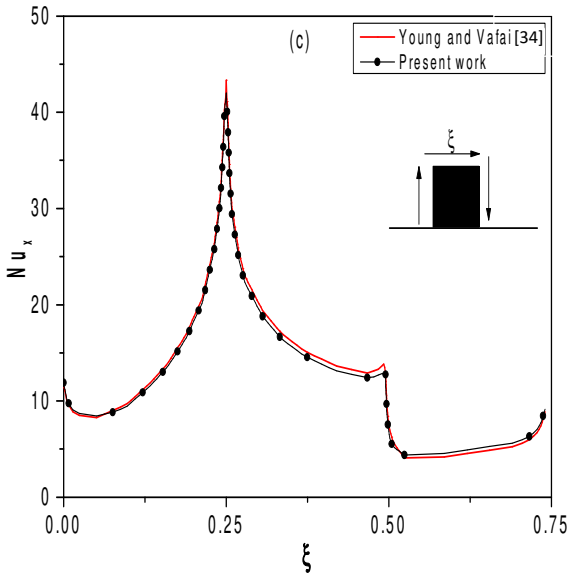

Fig. 2: Computation validation by comparison with the results of Young and Vafai [34, 35]: (a) streamlines, (b) obstacle surface temperature and (c) local Nusselt number.

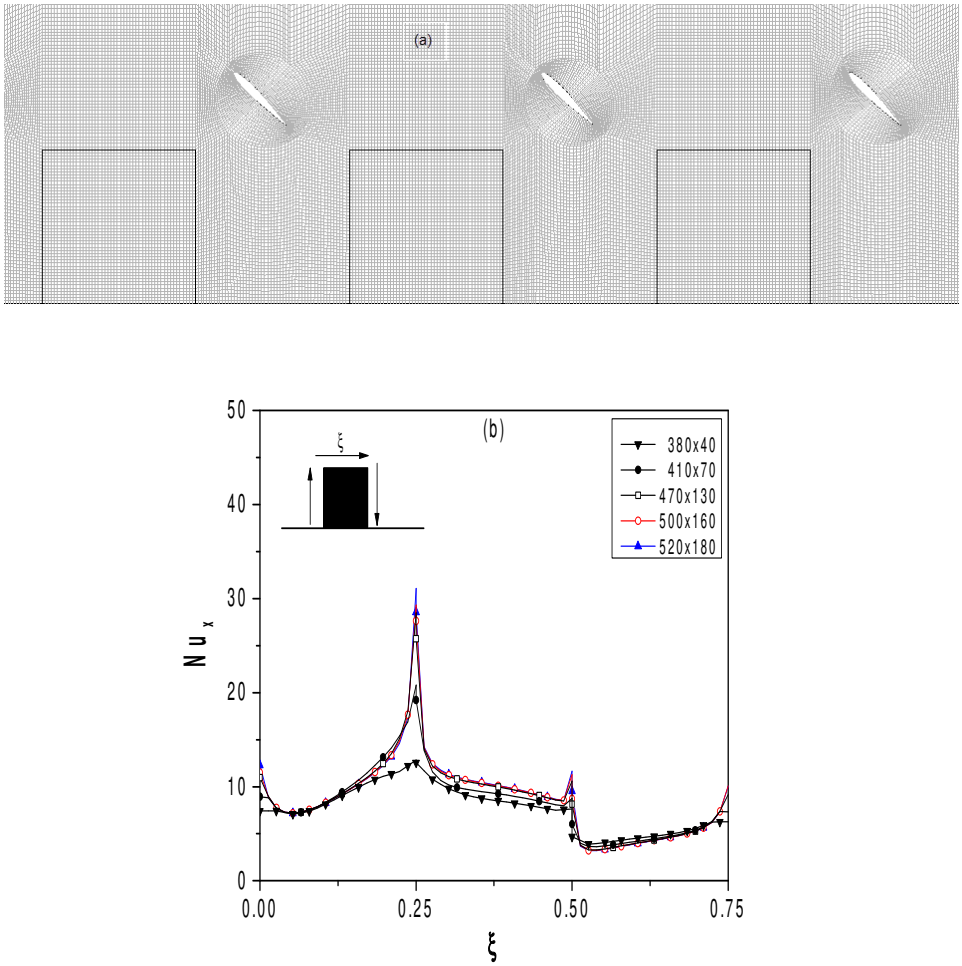

Fig.3: Grid independence: **(a)** detail of the mesh whose size is 500x160 for the whole domain around 5 blocks (**b)** *Nusselt* number according to different grid sizes**.**

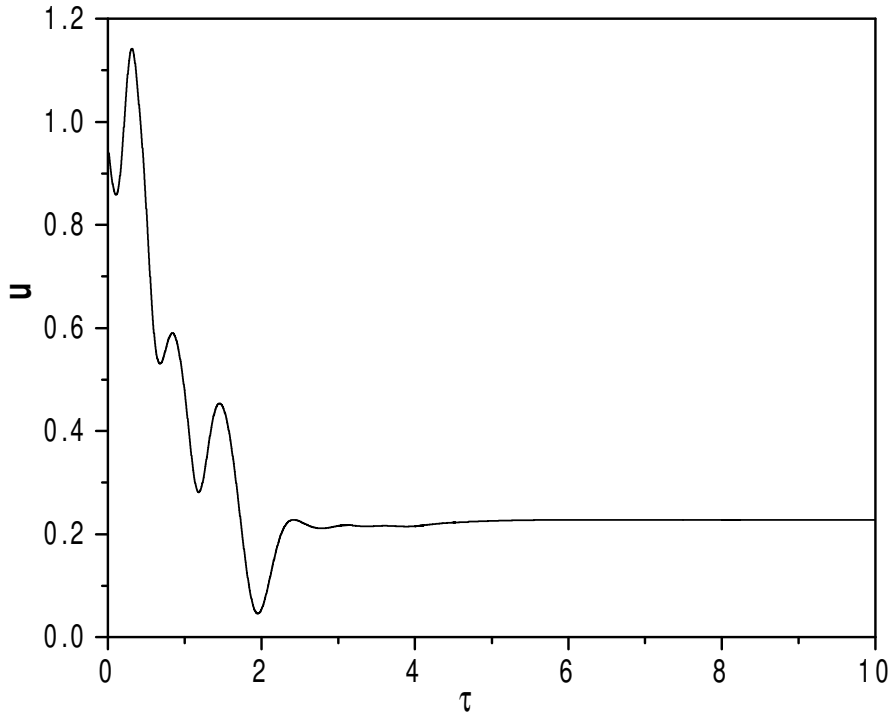

Fig. 4: The u-velocity component history at the reference point (x=4.875, y=0.250) for Re=500.

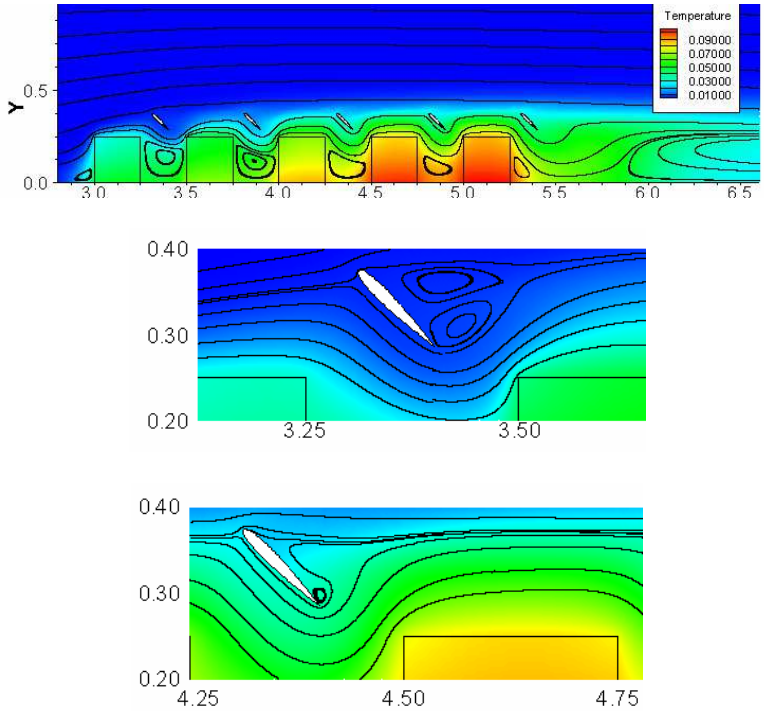

Fig. 5: Streamlines with isotherms field (back colour) for Re=500.

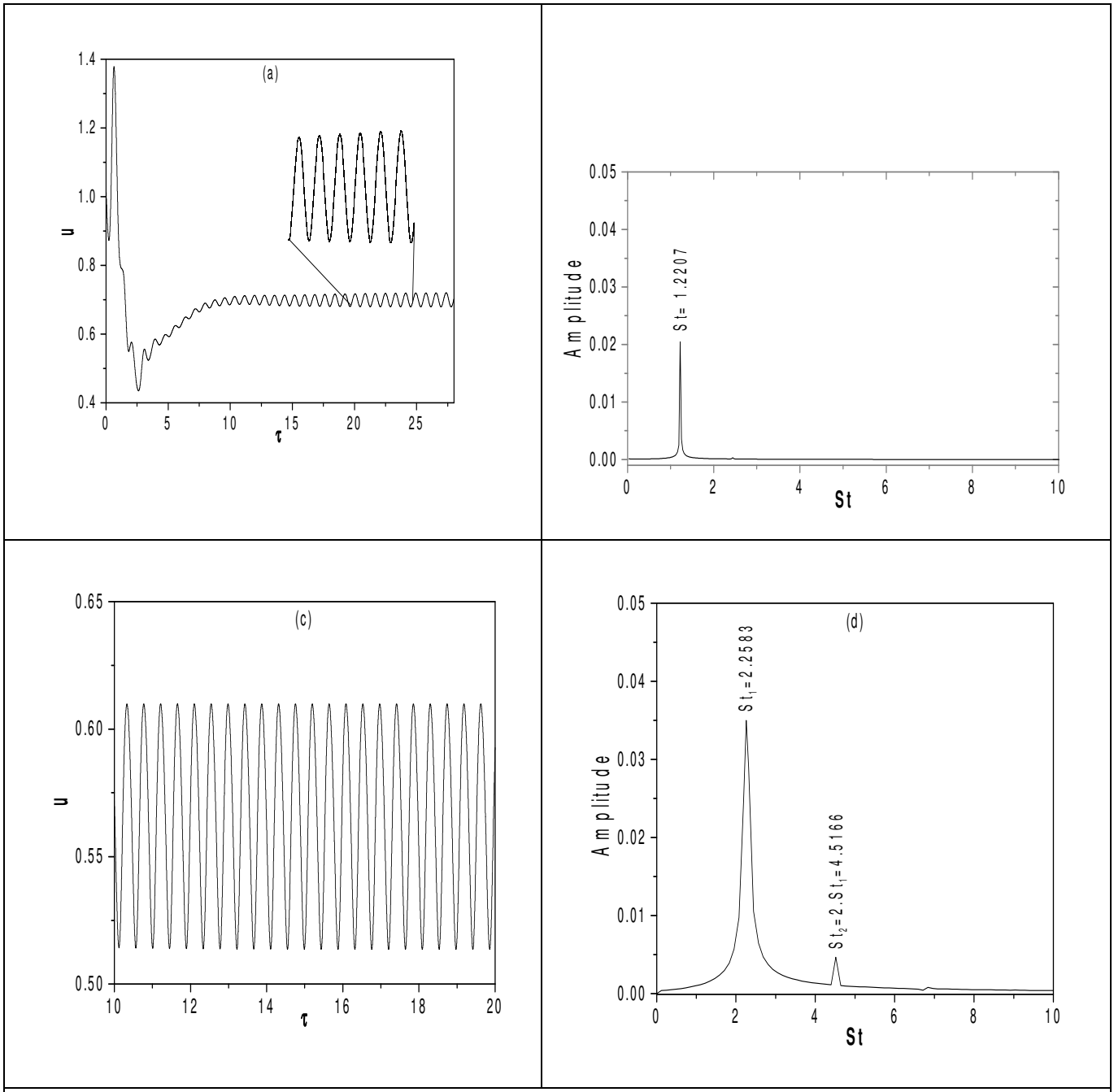

Fig. 6: The u-velocity component history at the reference point (x=4.875, y=0.250) and the FFT analysis for Re=1000 (a and b) and Re=1800 (c and d), respectively.

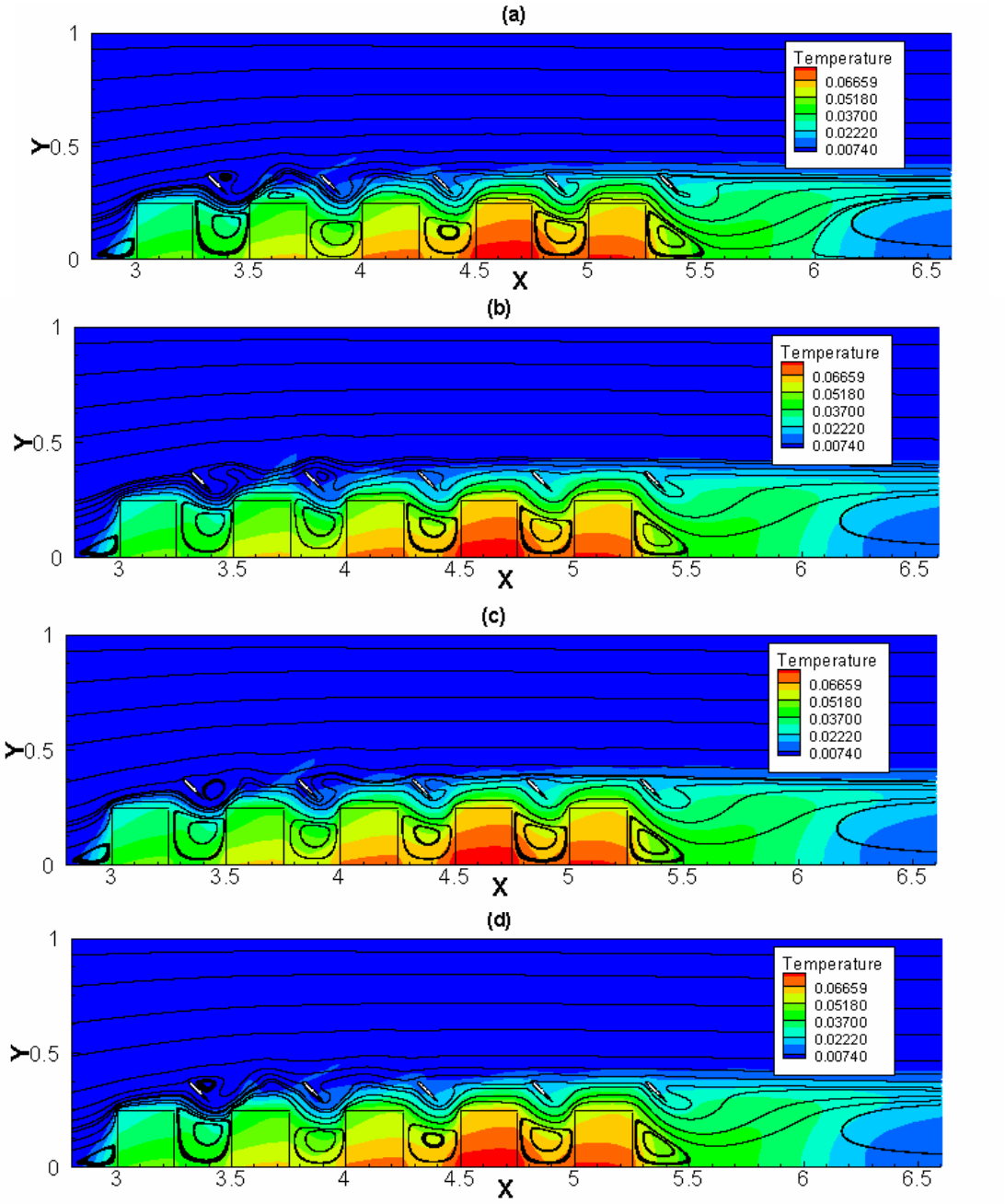

Fig. 7: Streamlines and isotherms contours during one time period for Re=1000: (a)τ, (b)$\tau+1/3\tau_p$, (c)$\tau+2/3\tau_p$, (d)$\tau+\tau_p$

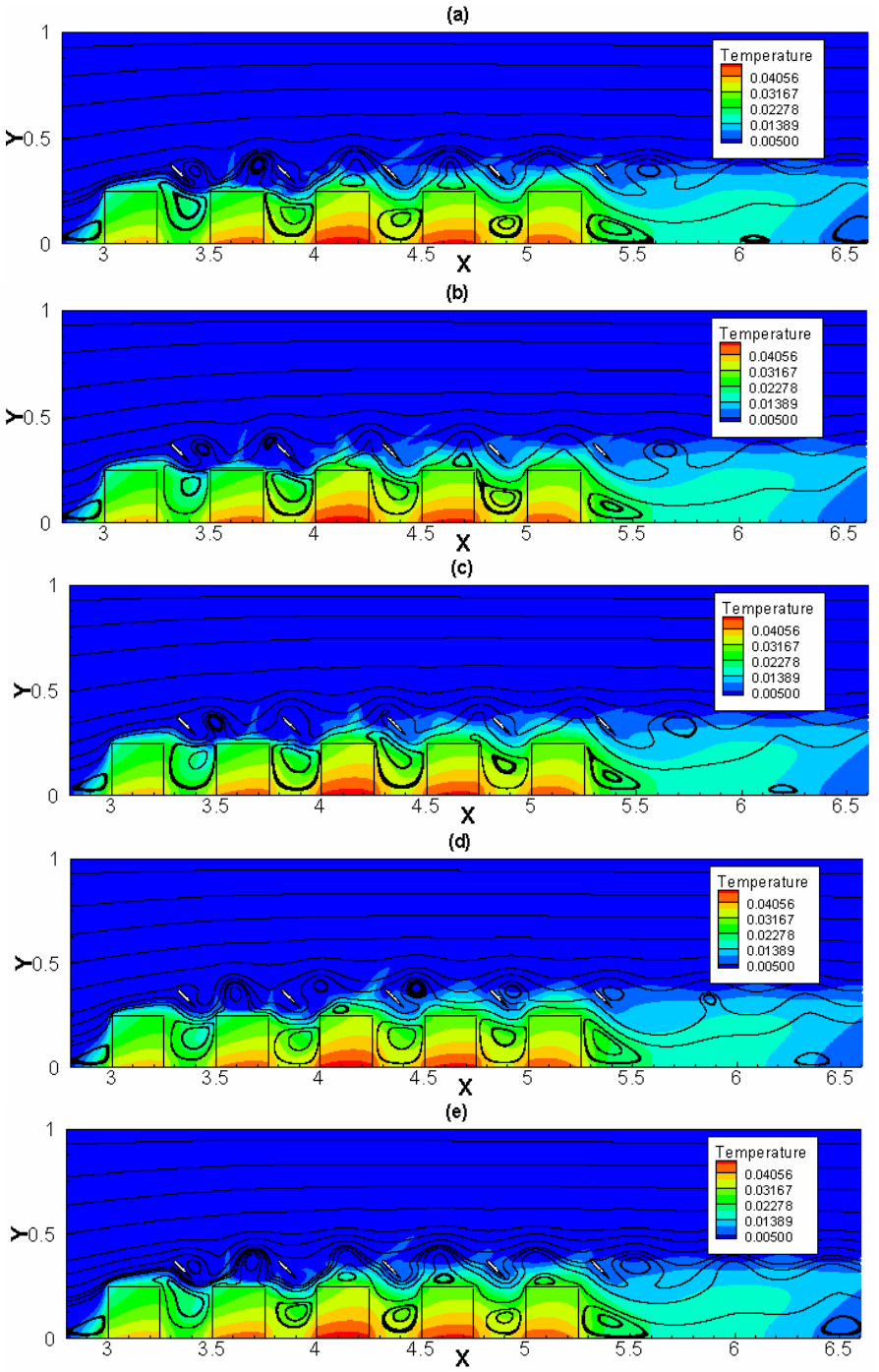

Fig. 8: Streamlines and isotherms contours during one time period for Re=1800: (a)τ, (b)$\tau+1/4\tau_p$, (c)$\tau+1/2\tau_p$, (d)$\tau+3/4\tau_p$, (e)$\tau+\tau_p$

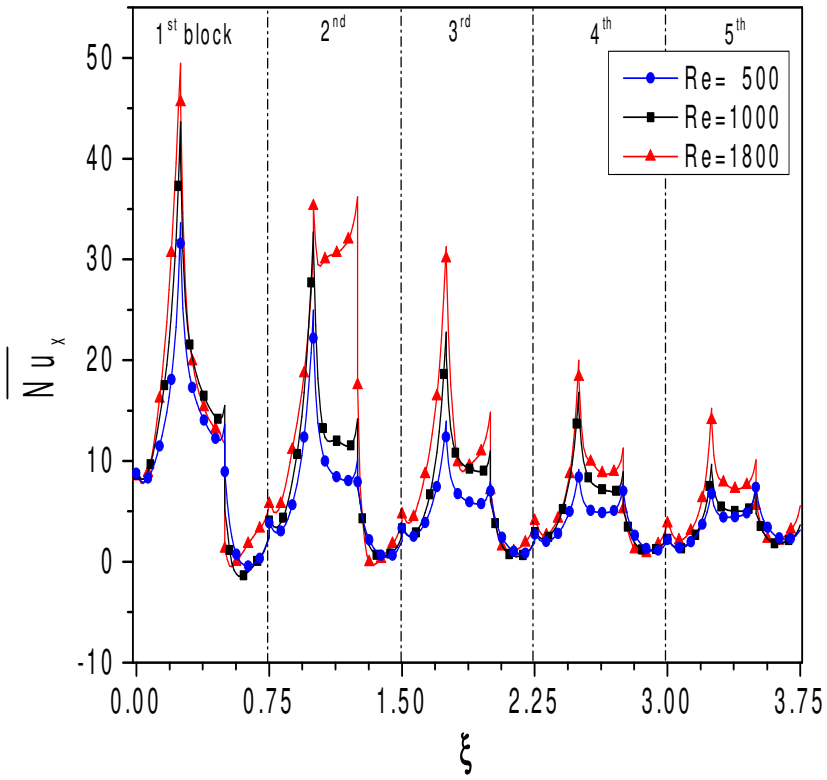

Fig. 9: Local Nusselt number evolution over the blocks peripheral distance for different Reynolds numbers.

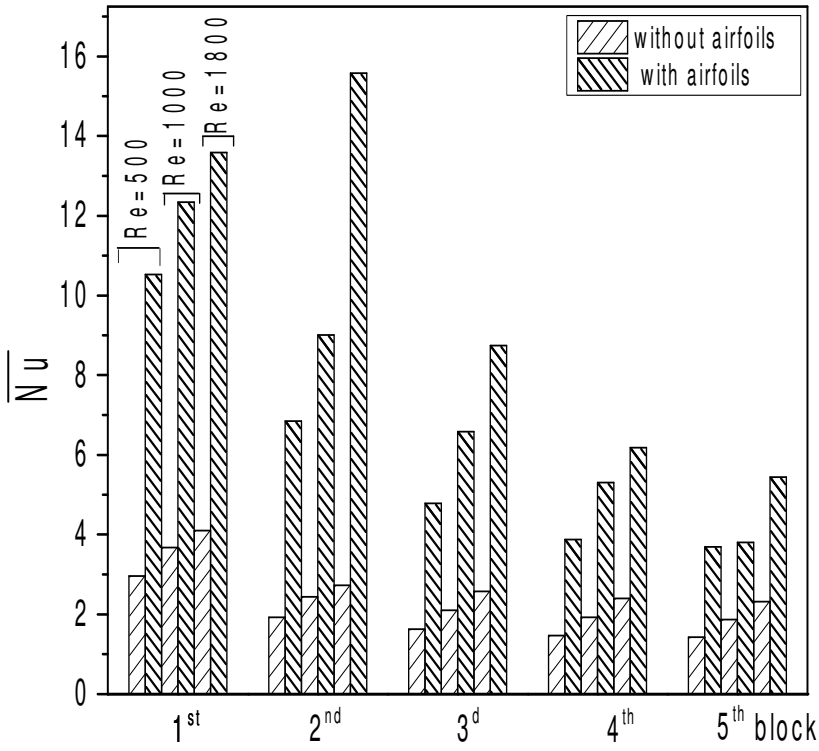

Fig. 10: Mean block Nusselt number with and without airfoils at different Reynolds number values.

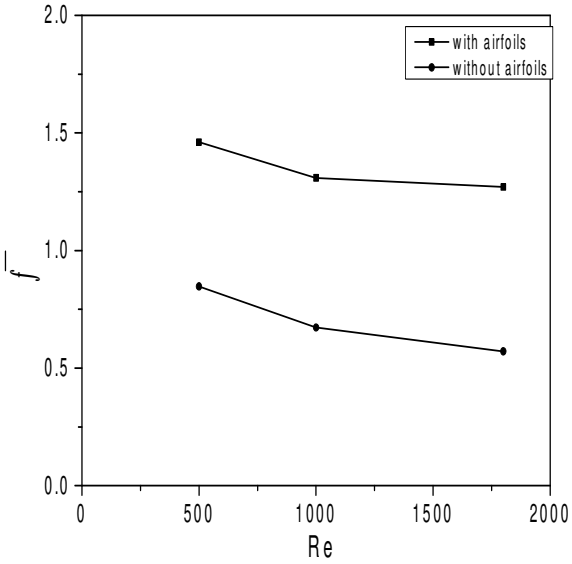

Fig. 11: Friction factor versus Reynolds number with and without airfoils

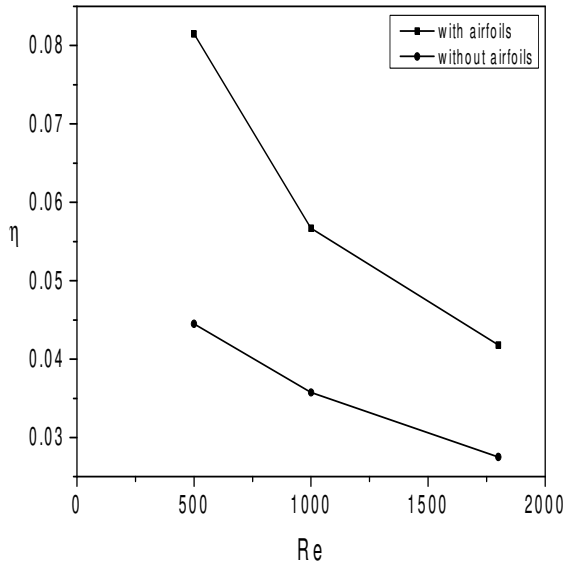

Fig. 12: Heat transfer efficiency vs. Reynolds number.

Tables:

Tab. 1: Strouhal number of the dominant frequency at various Reynolds number values.

Re	1000	1500	1800	2000
St	1.2207	2.3193	2.2583	2.1973

Tab. 2: Heat transfer augmentation at various Reynolds number.

Re	$\frac{(Nu_{with\ airfoil} - Nu_{without})}{Nu_{without}}\%$
500	215
1000	208
1800	258